# Hybrid plasmonic gold-nanorod–platinum short-wave infrared photodetectors with fast response

Hengyang Xiang, Zhelu Hu, Laurent Billot, Lionel Aigouy, Zhuoying Chen

DOI: 10.1039/c9nr04792a

# Hybrid Plasmonic Gold-Nanorod-Platinum Short-Wave Infrared Photodetectors with Fast Response

Hengyang Xiang, Zhelu Hu, Laurent Billot, Lionel Aigouy[#], Zhuoying Chen*

Short-wave infrared (SWIR) photodetectors, sensitive to the wavelength range between 1 and 3 μm, are essential components for various applications, which constantly demand devices with a lower cost, a higher responsivity and a faster response. In this work, a new hybrid device structure is presented for SWIR photodetection composing a coupling between solution-processed colloidal plasmonic gold (Au) NRs and a morphology-optimized resistive platinum (Pt) microwire. Pt microwires harvest efficiently the photothermal effect of Au NRs and in return generating a change of device resistance. A fast photon-heat-resistance conversion happens in these Au-NRs/Pt photodetectors exhibiting a response (rise) time of 97 μs under the illumination of a λ = 1.5 μm laser. Clear photoresponse can be observed in these devices at a laser illumination with a modulation frequency up to 50 kHz. The photoresponsivity of the current devices reached 4500 Ω/W under a laser power of 0.2 mW, which is equivalent to a responsivity of 340 mA/W under a DC bias of 1V. A series of mapping experiments were performed providing a direct correlation between Au NRs and the device zone where resistance change happens under a laser illumination modulated at different frequencies.

## Introduction

Short-wave infrared (SWIR) photodetectors, sensitive to the wavelength range between 1 and 3 μm, are essential components for various applications such as optical communication, image sensors, passive night vision, environmental gas sensing, spectrometry, biodiagnostics and artificial intelligence (AI).[1–5] Intensive efforts are currently underway to achieve SWIR photodetectors with low-cost, high-responsivity and fast-response that are necessary for new applications. For example, in the field of Lidar (Light Detection and Ranging), there is a strong quest for low-cost photodetectors sensitive to the wavelength of 1.5 μm, a wavelength allowing for a much longer detection distance compared to current technologies.[6] Most current Lidar devices that apply silicon sensors (band gap = 1.1 eV) can detect a distance up to about 100 m due to the eye-safe restrictions of the laser operating power. By comparison, if a laser with a wavelength of 1.5 μm can be used, a much higher laser power is allowed thus leading to a longer detection distance.[7,8] Unfortunately, most current photodetectors that are capable to detect λ = 1.5 μm photons (such as III-V InGaAs and or HgCdTe systems) are both costly and environmentally unfriendly due to their epitaxial growth requirements and the use of highly toxic elements. Indeed, high-performance SWIR photodetection have been realized by Ge-on-silicon fabricated by E-beam evaporation[9] and chemical vapor deposition.[10,11] Yet, alternative SWIR photodetection strategies, in particular solution-processed ones, should favor the further development of this field.

There have been therefore much research efforts longing for cost- and performance-competitive SWIR photodetection alternatives over the current III-V InGaAs or HgCdTe technologies. Towards this goal, many new materials have been proposed, including black phosphorus,[12,13] graphene,[14–17] $MoS_2$,[18] and colloidal PbS nanocrystals.[2,19] They show great promise in terms of operation at high modulation frequencies or high sensitivity. But some disadvantages still keep them away from the market: rigorous production process (poor reproducibility), non-adaptability to scale-up fabrication, manufactory safety and security concerns (due to the use of highly toxic elements).[20–22] Alternatively, solution-processed plasmonic metal nanoparticles, such as colloidal gold nanorods (Au NRs), exhibit interesting characteristics possible to overcome these disadvantages: capability of scaling-up synthesis, solution-processability adaptable to low-cost fabrication, high stability, low biological toxicity, and large optical absorption cross-section for SWIR photons.[23–27] The large absorption cross-section of originates from the localized surface plasmon resonance (LSPR) excitation, which decays through landau damping generating hot carriers on a time scale from 1 to 100 fs.[28] The fate of these hot carriers, if not being extracted by a specific device structure, is rapid heat generation and transferred to the surroundings on the ps-ns time-scale. Colloidal plasmonic metal nanoparticles are thus an efficient medium capable to convert received photons to heat. While such photon-heat conversion capability (or termed "photo-thermal effect") of plasmonic nanoparticles have been explored in photocatalysis[29,30] and cancer therapy,[31–33] its application on photodetection is still rare.[34] In particular, previously reported commercial thermistors applying the photothermal effect of Au NRs exhibited only slow response (rise/decay time = ~ 2 s) which was limited by the response time of the thermistor itself.[34]

In this work, we propose a new hybrid SWIR photodetector, based on the coupling between a morphology-optimized resistive platinum (Pt) microwire and colloidal plasmonic Au NRs, capable to reduce the photoresponse time of more than

four orders of magnitudes compared to previous study. Pt was chosen here due to its large temperature coefficient of resistance, wide operation temperature range, high stability and repeatability. The combination of these characteristics has led to the extensive applications of Pt as a resistance temperature detector (RTD).[35–38] Here a series of Pt microwires of various dimensions were fabricated and applied to harvest the photothermal effect of Au NRs. In an optimized Au-NRs/Pt photodetector, we measured a response time of 97 µs under the illumination of a λ = 1.5 µm laser with its ON/OFF modulated at 120 Hz. Remarkably, even at an illumination modulation frequency of 50 kHz, such Au-NRs/Pt photodetectors are still capable to generate clear photoresponse switching. The measured photoresponsivity of the current devices reached 4500 Ω/W under a laser power of 0.2 mW, which is equivalent to a responsivity of 340 mA/W under a DC bias of 1V. These hybrid Au-NRs/Pt photodetectors, capable to provide a fast conversion between SWIR photons, heat, and resistance change at a frequency up to tens of kHz, thus represent a brand-new strategy for SWIR photodetection alternatives, meeting the needs of emerging applications demanding reduced fabrication cost and high operation speed.

## Experimental

### Pt microwire RTD devices

Quartz coated glass substrates were cleaned by ultrasonication in a bath of de-ionized (DI) water, acetone and 2-propanol followed by $O_2$ plasma etching. A layer of adherence promoter (TI from microchemicals) and a layer of photosensitive resin (AZ5214, microchemicals) were spin-coated one after the other on these glass substrates. Pt microwires of various dimensions were then defined by direct laser writing lithography (Heidelberg Ins. laserwriter µPG101). Substrates were then developed by dipping the sample in a bath of developer (AZ726 MIF, microchemicals) for 30 s with subsequent DI water rising and air-drying. A Ti (5 nm)/Pt (40 nm) layer was then evaporated onto the sample by an e-beam evaporator (Plassys MEB550S). Finally, the Pt-coated substrates were lifted-off by immersing the samples into a bath of acetone.

### Optical and morphology characterizations

UV-Visible absorption spectra were measured in air by an Agilent 5E UV-Visible-NIR spectrometer. TEM characterizations were performed by a JEOL 2010 microscope operated at 200 kV. SEM characterizations were performed by a FEI Magellan 400 system with a field emission gun electron source.

### Au NRs/Pt hybrid photodetectors

Colloidal Au NRs with an aspect ratio of 10.96 were synthesized by a previously described method.[34] A drop (1 µL) of Au NR solution in water (with an optimized concentration of 4.8 g/L) was casted directly onto the surface of the Pt microwire and allowed to dry. For device measurement, a Fabry-Perot pigtailed laser ($\lambda_{peak}$ = 1.537 µm) was focused at oblique incidence at a 10-µm-diameter spot onto the sample. The time-dependent photoresponse characteristics (in terms of resistance change) was measured by a computer-controlled Keithley 2634B source measurement unit under a DC bias (0.01 V for 10-µm, 20-µm, 30-µm and 150-µm-long devices, 0.2 V for 1500-µm-long devices). To characterize the response speed of the device under different illumination modulation frequencies

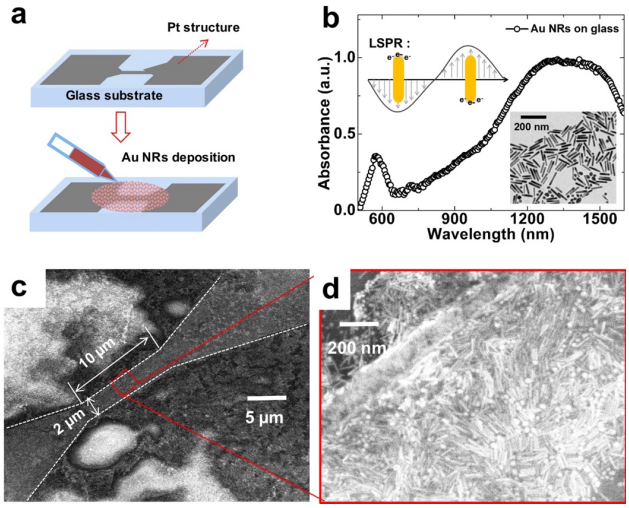


**Figure 1.** (a) Schematic of the deposition of a drop (1 µL) of Au NR solution onto the surface of a Pt microwire RTD. (b) Optical absorbance spectrum of a film of Au NRs on a glass substrate (the upper inset shows a schematic of the longitudinal surface plasmon resonance (LSPR) of Au NRs; the lower inset shows a TEM image of these Au NRs). (c) SEM image of a typical Au-NRs/Pt device. (d) Zoom-in SEM image permitting visualisation of the Au NRs on the surface of a Pt microwire.

(100 Hz, 1 kHz and 20 kHz), the device was put into a circuit where an external voltage of 0.1 V was applied and a current-limiting resistance (207 Ω) was placed in series with the device under test. The voltage drop onto the device was amplified by a low-noise preamplifier (Stanford Research System SR560) and measured by an oscilloscope (Tektronix DPO2024B). The measured voltage change ΔV (under illumination) is proportional to ΔR (ΔR ≈ 5513.79•ΔV). The mapping experiments under a laser illumination of various modulation frequencies and the frequency responses on a continuous spectral range were measured on the device in the above-mentioned circuit by a lock-in amplifier (EGG7260 DSP). For mapping experiments, the device position was controlled by a XYZ piezoelectric stage.

## Results and discussion

A series of Pt microwires of different lengths (from 1.5 mm to 10 µm) and widths (from 200 µm to 2 µm) were defined by photolithography on quartz coated glass substrates. These Pt microwires serve as the resistance temperature detectors (RTD) to harvest the photothermal effect of colloidal Au NRs. Au NRs dispersed in water with an optimized concentration (4.8 g/L) was then deposited onto the surface of a Pt RTD. The preparation process is described in Figure 1a and in the experimental section. The optical absorbance of Au NRs deposited on a glass substrate exhibits a strong absorption in the wavelength range between 1200 nm and 1600 nm (Figure 1b) which originates from the longitudinal surface plasmon resonance (LSPR) of these high aspect-ratio Au NRs. As observed in transmission electron microscopy (TEM) characterizations (insert of Figure 1b), these Au NRs are relatively monodisperse

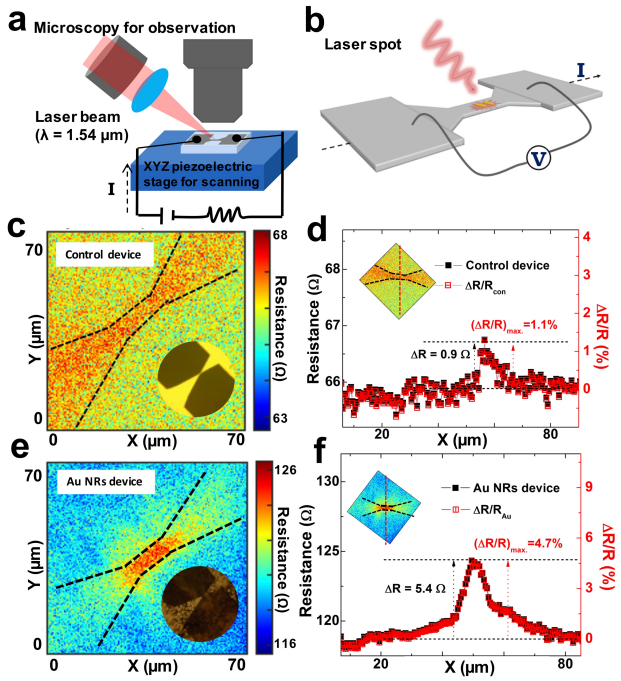


**Figure 2.** (a) Schematic of the experimental set-up and the circuit used for device measurement; An external voltage of 0.1 V was applied and a current-limiting resistance (207 Ω) was placed in series with the device under test. (b) Schematic of the device where the voltage fell onto it was measured and the change of it (ΔV) is proportional to ΔR. (c) and (e) Resistance mappings of the control device without Au NRs (c) and the Au-NRs/Pt device (e) under a 10-μm-spot continuous laser illumination (λ = 1.5 μm) while the sample position was controlled by a piezoelectric stage. (d) and (f) The cross-sectional profiles extracted from the mapping images shown in (c) and (e) and the resultant device response in terms of ΔR or ΔR/R of the control device (d) and the Au-NRs/Pt device (f).

with an average rod length of 94 ± 13 nm, an average diameter of 8.5 ± 1.5 nm, giving an aspect-ratio of ~ 11. Scanning electron microscope (SEM) characterizations were carried out on a typical Au-NRs/Pt device (Figure 1c and 1d) revealing a dense layer of Au NRs on the Pt microwire RTD.

To explore the interaction between SWIR photons and the hybrid Au-NRs/Pt devices, a homebuilt microscope[39,40] was applied where an Au-NRs/Pt device was illuminated by a λ = 1.5 μm laser spot (diameter of ~ 10 μm) while the device position was controlled by a piezoelectric stage during a scanning experiment. As a function of the laser position on the device surface, the resistance of the device was analyzed by measuring the voltage fell on the device under a circuit shown in Figure 2 with an external applied voltage of 0.1 V. Under identical experimental conditions, such scanning experiments were performed under a continuous laser illumination with a power density of 80 μW/μm$^2$ respectively on a control device (Pt microwire without Au NRs) and an Au-NRs/Pt device (Pt microwire covered by Au NRs) where the Pt microwire has a dimension of 10 μm by 2 μm (below termed as "10-μm devices"). The resistance mapping obtained in such scan experiments (Figure 2c and 2e) exhibits a clear profile identical to the morphology characterization of the Pt microwire by SEM shown in Figure 1c. By comparison to the control device, the observed resistance change under illumination in the Au-NRs/Pt device occurs mainly at the Pt microwire (where the resistance is large) but not at the large contact pads. A more pronounced resistance contrast was observed, indicating a drastic increase of resistance in the Au-NRs/Pt device under laser illumination likely due to the plasmonic-induced photothermal effect of the Au NRs covering the surface of the Pt microwire: Upon absorption of the laser illumination, Au NRs generate heat and transfer it to the Pt microwire whose resistance is highly sensitive to any temperature change. By comparison, even though there is heat generated on the control device under the same laser illumination, such amount of heat is too small to generate a significant change of resistance. To quantify the difference between the Au-NRs/Pt device and the control device, the resistance line profiles across a device obtain from the mapping experiments are compared (Figure 2d and 2f): Here, the change of resistance due to laser illumination normalized by the device resistance in dark (ΔR/R = ($R_{laser}$-$R_{dark}$)/$R_{dark}$) represents the measurable output of this type of photodetectors at a certain laser power. Note that there was a slight difference in the absolute value of the dark resistance of the two devices, which is likely due to the existence of colloidal Au NRs coating on the Au-NRs/Pt device and any possible (resistive) surfactant residue from the synthesis. Remarkably, the ΔR/R observed in the Au-NRs/Pt device (ΔR/R = 4.7%) is more than four-fold larger than that observed in the control device (ΔR/R = 1.1%). Clearly, the existence of Au NRs on the surface of Pt microwire and their photothermal effect boosted the responsivity of the device.

Not only being able to provide a clear photoresponse in the form of resistance change under the λ = 1.5 μm laser illumination, these Au-NRs/Pt hybrid devices also exhibit fast-switching sensing capabilities at high illumination modulation frequency. The time-dependent photoresponse of a typical 10-μm Au-NRs/Pt device under a modulated laser illumination at various frequencies is shown in Figure 3. At low laser (λ = 1.5 μm) modulation frequency (Figure 3a-3c), nearly instantaneous rise/fall of the device resistance was observed at different laser powers (from 0.2 mW to 1.6 mW, corresponding to a power density ranging from 10 μW/μm$^2$ to 80 μW/μm$^2$, Figure 3a). In particular, even under a very low laser power (0.2 mW, 10 μW/μm$^2$), the Au-NRs/Pt device is still capable to generate a clear resistance change (Figure 3a, dark curve) while only negligible resistance change was observed in the control device under the same condition. The photoresponsivities of both the Au-NRs/Pt device and the control device are shown in Figure 3b, represented by either the change of resistance ΔR normalized by the laser power (P), *i.e.* ΔR/P in the unit of Ω/W, or (ΔR/R)/P in the unit of %/W). The photoresponsivity of the current Au-NRs/Pt device increased roughly linearly as the laser power reduces (Figure S2). This is likely due to the change of thermal properties of the Pt microwire and/or the saturation of optical absorption of Au NRs at high laser power. Please note that the current photodetectors are resistive devices. Therefore, the presented photoresponsivity of this work is different from those of a photoconductive or photovoltaic device on which the

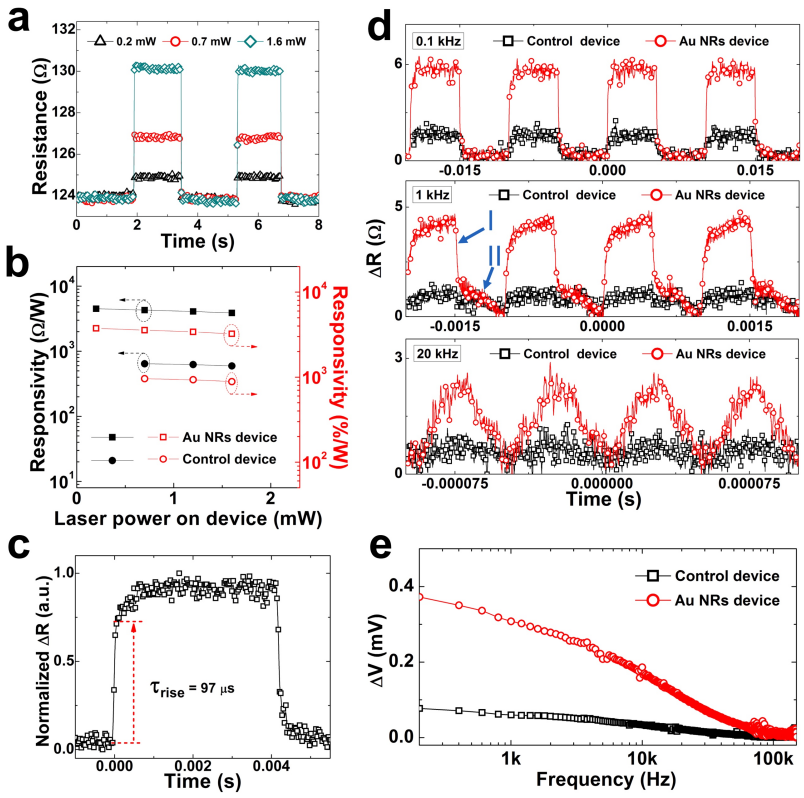


**Figure 3.** (a) Time-dependent photoresponse characteristics of a 10-μm Au-NRs/Pt device as a function of laser power (0.2 mW, 0.7 mW and 1.6 mW, corresponding to a density of 10 μW/μm$^2$, 35 μW/μm$^2$ and 80 μW/μm$^2$, λ = 1.5 μm). (b) The photoresponsivity (in terms of R/P (Ω/W) or (ΔR/R)/P (%/W), P = laser power) of the Au-NRs/Pt device at different laser powers. (c) Zoom-in time-dependant photoresponse characteristics permitting the extraction of the device response speed (rise/decay profile) under a laser illumination modulated at 120 Hz. (d) Comparison of the photoresponse characteristics from the Au-NRs/Pt and the control device under a λ = 1.5 μm laser illumination modulated at different frequencies: 0.1 kHz, 1 kHz and 20 kHz. (e) Evolution of the photoresponse as a function of laser modulation frequency from 200 Hz to 150 kHz for both the control and Au-NRs/Pt device.

photoresponsivity is typically given by the change of measured photocurrent (ΔI) normalized by the laser power (P), *i.e.* ΔI/P in the unit of A/W. Under a laser power of 0.2 mW, the measured photoresponsivity of the current devices reached 4500 Ω/W (Figure 3b), which is equivalent to a responsivity of 340 mA/W under a DC bias of 1V (Figure S2). By comparison to the control device, about four-fold responsivity enhancement was observed in the Au-NRs/Pt device under different applied laser powers, except for the case of the lowest laser power (0.2 mW) where the control device exhibited no photoresponse under the same measurement condition. The wavelength dependence of the change of resistance (ΔR) of an Au-NRs/Pt device is shown in Figure S3. In terms of response time of such Au-NRs/Pt device, it can be extracted from Figure 3c that provides a zoom-in view of the rise/decay profile following a laser illumination operated at 120 Hz. Defined as the time used by the resistance to increase from null to 80% of the saturation level, the response time of this device is measured as 97 μs, which is more than four orders of magnitudes smaller than the response time measured in a previous work.[41] Such rapid photoresponse originates from both the efficient heat transfer between Au NRs and the Pt microwire and the optimized geometry of the Pt microwire. Indeed, as the dimension of the laser spot applied in this work is about 10 μm, a 10-μm-long Pt microwire can be fully illuminated by the laser spot without the laser spot shining onto the large contact pads. If a shorter Pt microwire is used with the laser spot covering the contact pads, a large amount of heat can be generated and thus a much longer time will be needed for the device to cool down (when the illumination is off) leading to difficulties in switching off the device. Beyond this optimized Pt microwire dimension, increasing either the length or the width of the Pt microwire led also to an increased device response time (Figure S1 and Table S1 in the Supporting Information). In the devices based on either a longer or wider Pt microwire, only a part of the microwire was illuminated by the laser and heat up by the Au NRs. A longer time is thus needed for these Pt microwires to reach a thermal equilibrium, leading to a longer rise/fall time. This observation is in agreement with numerical simulations on Joule-heated nanowires[42] which show a longer response time along with an increased nanowire dimension.

The fast-response time of the optimized Au-NRs/Pt device thus allows their operation at a higher laser modulation frequency. The time-dependent photoresponse in terms of resistance change (ΔR) of the Au-NRs/Pt device under a laser illumination

(λ = 1.5 μm) with ON/OFF modulated at 0.1 kHz, 1 kHz and 20 kHz is shown in Figure 3d. At all measured frequencies, a clear enhancement of photoresponse can be observed in the Au-NRs/Pt device compared to the control device. From the photoresponse decay characteristics of the Au-NRs/Pt device (e.g. Figure 3d, at 1 kHz), one can notice that there was two decay stages: "stage I" for a fast decay and "stage II" for a much longer decay. In particular, one can observe that the data of stage II (red open circles) overlap closely with those from the control device (black open squares). Therefore, while the exact origins of these two stages are not well-known, we speculate that they might come from that fact that Au NRs did not fully cover 100% of the Pt microwire. As a result, the uncovered part of the device exhibited a similar decay behavior as the control device, contributing to the coexistence of two different decay stages. As modulation frequency increases, the time-dependent resistance change (ΔR) starts to deviate from the rectangular form of the laser modulation. Nevertheless, even at 20 kHz, in contrast to the control device, the Au-NRs/Pt device is still capable to provide a clear photoresponse switching. By a lock-in amplifier, the peak-to-peak voltage variation ΔV (V) measured on the Au-NRs/Pt device and the control device (in both cases proportional to ΔR) as a function of the modulation frequency of the laser beam in a continuous spectral frequency range (from 200 Hz to 150 kHz) is exhibited in Figure 3e. Even at 50 kHz, the Au-NRs/Pt device still exhibited a response amplitude of 40 μV, which is more than 10% of that measured at low frequency (ΔV = 370 μV at 200 Hz). Compared to the control device, the Au-NRs/Pt device exhibited a response more than four times larger than that of the bare Pt control device on the whole frequency range, which is coherent as the observations shown in Figure 2d and 2f. Similar results were also obtained on Au-NRs/Pt devices based on a Pt microwire with a length of 20 μm or 30 μm (termed as 20-μm or 30-μm devices, Figure S4).

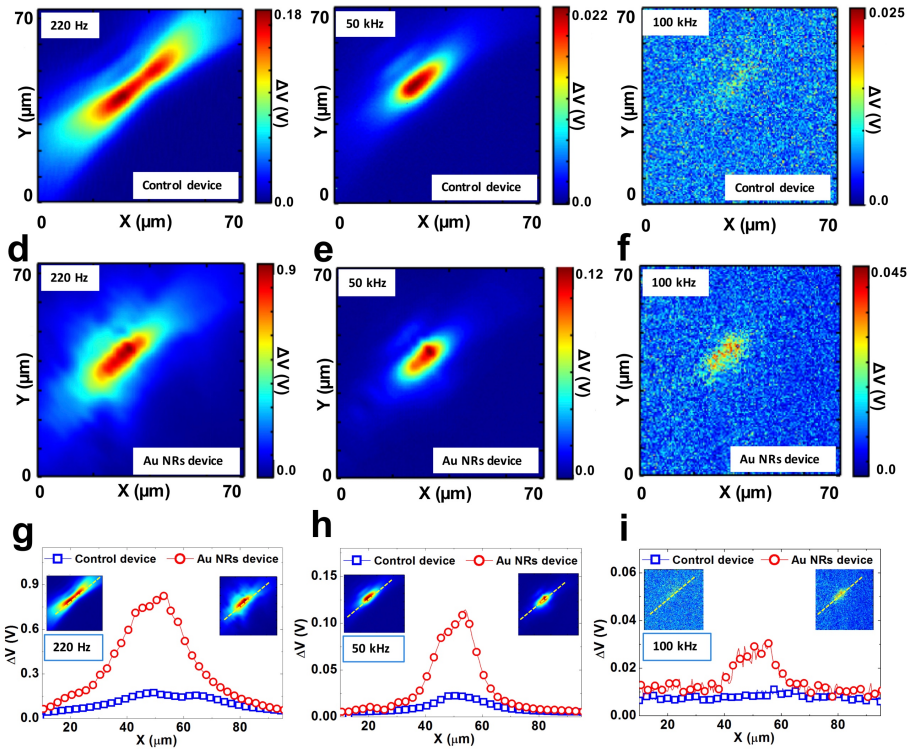


**Figure 4.** Mapping of the voltage change measured on the control device (a-c) and the Au-NRs/Pt device (d-f) in the circuit described in Figure 2 under a 10-μm-spot of λ = 1.5 μm laser modulated at 220 Hz (a, d), 50 kHz (b, e) and 100 kHz (c, f). Note that the measured ΔV is proportional to ΔR. (g-i) The cross-sectional profiles extracted from the mapping images with the illumination modulated at 220 Hz (g), 50 kHz (h) and 100 kHz (i).

**Table 1.** Summary of the response time of the photodetectors applying colloidal plasmonic metallic nanoparticles.

| Device structure | Wavelength | Response time | Ref. |
|---|---|---|---|
| Au NPs/$TiO_2$ | 400-900 nm | 1.5 s | [43] |
| Au NRs/ZnO Nanowire | 650-850 nm | 0.25 s | [44] |
| Au NPs/Graphene | 532 nm | 1.5 s | [45] |
| Au NRs/NTC thermistor | 1.0-1.8 μm | 2.5 s | [34] |
| Au NRs/Pt | 1.5 μm | 97 μs | this work |

In order to visualize how the laser modulation frequency affects the location of the resistance change, we then performed mapping experiments on the ΔR of the device with a modulated laser. During such mapping experiments, the device position was controlled by a piezoelectric stage. In contrast to the mapping experiments shown in Figure 2 under a continuous laser illumination, here, several frequencies (220 Hz, 50 kHz and 100 kHz) were applied to modulate the laser ($\lambda$ = 1.5 μm) illumination. At each frequency, the illumination-induced (peak-to-peak) voltage change was measured as a function of the position of the laser beam on the device by a lock-in amplifier with a gain of 2000. These mapping experiments thus give a direct proof of device functioning under various laser modulation frequencies. Results obtained on the control and the Au-NRs/Pt devices are shown in Figure 4a-c and 4d-f, respectively. For both devices, as the frequency increases, the device responsivity decreases, which is coherent with the observation shown in Figure 3e. For the control device, the light modulation induces a resistance change that extends to the contact pads at low frequency (Figure 4a). As the frequency increases, the zone that corresponds to the resistance change shrinks down to within the microwire (Figure 4b). This behavior can be explained by the fact that, at low frequency, the device has the time to heat up and cool down to a larger area within a modulation cycle. This is no more the case at higher frequency where the temperature stabilizes at an average value and only the microwire region is small enough to follow the heating and cooling sequence. The same behavior is observed on the Au-NRs/Pt device, with a smaller device zone that corresponds to the resistance change as the frequency increases (Figure 4d, 4e and 4f). The normalized voltage drop for different frequencies allowing the comparison on its spatial distribution is shown in Figure S5. By comparison to the control device, at a given frequency, the Au-NRs/Pt device exhibits a more than four-fold stronger response (Figure 4g - 4i), which is coherent with the observations shown in Figure 2 and 3. In addition, at a given frequency, the zone that corresponds to the resistance change in the Au-NRs/Pt device is more localized than that in the control device. This is likely due to the non-uniform distribution (clustering) of the Au NRs on the Pt microwire contributing to a smaller heating zone.

These above results demonstrate that the Au-NRs/Pt device is capable to detect $\lambda$ = 1.5 μm photons and can function at up to a few tens of kilohertz of illumination modulation frequency. Surprisingly, compared to the numerous applications in photocatalysis[29,30] and cancer therapy,[46–49] in the field of photodetection, the photothermal effect of plasmonic nanoparticles has been rarely applied.[41] Instead, many previous reports applied colloidal plasmonic metal nanoparticles in the photodetector device either by harvesting the hot electrons generated ("hot-electron" devices)[43,44,50] or by benefiting from the plasmonic-enhanced light-harvest in the absorber of the device.[45,51,52] The characteristics in terms of operation wavelengths and response speed of some representative studies applying colloidal plasmonic metallic nanoparticles for the purpose of photodetection are summarized in Table 1 together with the results from this work. Remarkably, the response speed of the current Au-NRs/Pt device is hundreds of times to even thousands of times faster than previous studies. In addition, compared to previous studies, the current Au-NRs/Pt device operates at the wavelength of 1.5 μm, on which low-cost Si photodetectors do not have sensitivity. As discussed in the introduction, the merits of the current proposed hybrid colloidal Au-NRs/Pt photodetectors include the possibility of large-scale synthesis and the solution-processability of colloidal Au NRs, as well as the absence of highly toxic heavy metal elements. The application of plasmonic-induced photothermal effect for SWIR photodetection is still in its infancy as the first demonstration appeared only a year ago.[34] While at this stage they cannot overperform existing technologies like III-V, Ge, or Graphene (some which has been developed since more than forty years),[53] the current work represents a promising alternative path towards the next-generation low-cost SWIR photodetection. In terms of the perspectives to further improve the performance of these hybrid Au-NRs/Pt devices, possible directions includes engineering methods to load more Au-NRs onto the Pt microwire, as well as the formation of modules including multiple arrays of Au-NRs/Pt devices.

## Conclusions

In summary, we proposed a new hybrid device structure harvesting the photothermal effect of colloidal plasmonic Au NRs to achieve low-cost SWIR photon detection by coupling these NRs with a morphology-optimized resistive Pt microwire. These Au-NRs/Pt photodetectors are capable to response with a rise time of 97 μs under the illumination of a $\lambda$ = 1.5 μm laser. Under a laser power of 0.2 mW, the photoresponsivity of the current devices reached 4500 Ω/W. Even at an illumination modulation frequency of 50 kHz, such Au-NRs/Pt photodetectors are still capable to generate clear photoresponse switching. A series of mapping experiments were performed permitting a direct visualization of the device zone where a resistance change of the device was provoked by

a laser illumination modulated at different frequencies. These hybrid Au-NRs/Pt hybrid photodetectors, exhibiting a fast response at a frequency up to tens of kHz, thus open a new pathway for low-cost SWIR photodetection technology.

## Conflicts of interest

There are no conflicts to declare.

## Acknowledgements

SEM characterizations performed were supported by the region Île-de-France in the framework of DIM Nano-K. H.X. acknowledges the China scholarship council (CSC) for Ph.D. thesis scholarship.

## References

1 F. H. L. Koppens, T. Mueller, P. Avouris, A. C. Ferrari, M. S. Vitiello and M. Polini, *Nat. Nanotechnol.*, 2014, **9**, 780–793.

2 R. Saran and R. J. Curry, *Nat. Photonics*, 2016, **10**, 81–92.

3 B. Siegmund, A. Mischok, J. Benduhn, O. Zeika, S. Ullbrich, F. Nehm, M. Böhm, D. Spoltore, H. Fröb, C. Körner, K. Leo and K. Vandewal, *Nat. Commun.*, 2017, **8**, 15421.

4 F. P. G. de Arquer, A. Armin, P. Meredith and E. H. Sargent, *Nat. Rev. Mater.*, 2017, **2**, 16100.

5 R. R. LaPierre, M. Robson, K. M. Azizur-Rahman and P. Kuyanov, *J. Phys. D. Appl. Phys.*, 2017, **50**, 123001.

6 A. Wehr and U. Lohr, *ISPRS J. Photogramm. Remote Sens.*, 1999, **54**, 68–82.

7 J. Hecht, *Opt. Photonics News*, 2018, **29**, 26–33.

8 B. Schwarz, *Nat. Photonics*, 2010, **4**, 429.

9 Y. Salamin, P. Ma, B. Baeuerle, A. Emboras, Y. Fedoryshyn, W. Heni, B. Cheng, A. Josten and J. Leuthold, *ACS Photonics*, 2018, **5**, 3291–3297.

10 D. Ahn, C. Hong, J. Liu, W. Giziewicz, M. Beals, L. C. Kimerling, J. Michel, J. Chen and F. X. Kärtner, *Opt. Express*, 2007, **15**, 3916.

11 A. Gassenq, F. Gencarelli, J. Van Campenhout, Y. Shimura, R. Loo, G. Narcy, B. Vincent and G. Roelkens, *Opt. Express*, 2012, **20**, 27297.

12 H. Du, X. Lin, Z. Xu and D. Chu, *J. Mater. Chem. C*, 2015, **3**, 8760–8775.

13 N. Youngblood, C. Chen, S. J. Koester and M. Li, *Nat. Photonics*, 2015, **9**, 247.

14 F. Xia, T. Mueller, Y. M. Lin, A. Valdes-Garcia and P. Avouris, *Nat. Nanotechnol.*, 2009, **4**, 839–843.

15 T. Mueller, F. Xia and P. Avouris, *Nat. Photonics*, 2010, **4**, 297–301.

16 S. Cakmakyapan, P. K. Lu, A. Navabi and M. Jarrahi, *Light Sci. Appl.*, 2018, **7**, 20.

17 P. Ma, Y. Salamin, B. Baeuerle, A. Josten, W. Heni, A. Emboras and J. Leuthold, *ACS Photonics*, 2019, **6**, 154–161.

18 Y. Xie, B. Zhang, S. Wang, D. Wang, A. Wang, Z. Wang, H. Yu, H. Zhang, Y. Chen, M. Zhao, B. Huang, L. Mei and J. Wang, *Adv. Mater.*, 2017, **29**, 1605972.

19 D. Kufer, I. Nikitskiy, T. Lasanta, G. Navickaite, F. H. L. Koppens and G. Konstantatos, *Adv. Mater.*, 2015, **27**, 176–180.

20 Y. Geng, S. J. Wang and J. K. Kim, *J. Colloid Interface Sci.*, 2009, **336**, 592–598.

21 F. Giustino and H. J. Snaith, *ACS Energy Lett.*, 2016, **1**, 1233–1240.

22 N. K. Noel, S. D. Stranks, A. Abate, C. Wehrenfennig, S. Guarnera, A. A. Haghighirad, A. Sadhanala, G. E. Eperon, S. K. Pathak, M. B. Johnston, A. Petrozza, L. M. Herz and H. J. Snaith, *Energy Environ. Sci.*, 2014, **7**, 3061–3068.

23 H. Chen, L. Shao, Q. Li and J. Wang, *Chem. Soc. Rev.*, 2013, **42**, 2679–2724.

24 V. Sharma, K. Park and M. Srinivasarao, *Mater. Sci. Eng. R Reports*, 2009, **65**, 1–38.

25 V. Amendola, R. Pilot, M. Frasconi, O. M. Maragò and M. A. Iatì, *J. Phys. Condens. Matter*, 2017, **29**, 203002.

26 J. Cao, T. Sun and K. T. V Grattan, *Sensors Actuators B Chem.*, 2014, **195**, 332–351.

27 P. Yang, J. Zheng, Y. Xu, Q. Zhang and L. Jiang, *Adv. Mater.*, 2016, **28**, 10508–10517.

28 M. L. Brongersma, N. J. Halas and P. Nordlander, *Nat. Nanotechnol.*, 2015, **10**, 25–34.

29 S. Mukherjee, F. Libisch, N. Large, O. Neumann, L. V. Brown, J. Cheng, J. B. Lassiter, E. A. Carter, P. Nordlander and N. J. Halas, *Nano Lett.*, 2013, **13**, 240–247.

30 J. Lee, S. Mubeen, X. Ji, G. D. Stucky and M. Moskovits, *Nano Lett.*, 2012, **12**, 5014–5019.

31 A. Espinosa, M. Bugnet, G. Radtke, S. Neveu, G. A. Botton, C. Wilhelm and A. Abou-Hassan, *Nanoscale*, 2015, **7**, 18872–18877.

32 D. Jaque, L. Martínez Maestro, B. del Rosal, P. Haro-Gonzalez, A. Benayas, J. L. Plaza, E. Martín Rodríguez and J. García Solé, *Nanoscale*, 2014, **6**, 9494–9530.

33 Y. Ju, H. Zhang, J. Yu, S. Tong, N. Tian, Z. Wang, X. Wang, X. Su, X. Chu, J. Lin, Y. Ding, G. Li, F. Sheng and Y. Hou, *ACS Nano*, 2017, **11**, 9239–9248.

34 H. Xiang, T. Niu, M. S. Sebag, Z. Hu, X. Xu, L. Billot, L. Aigouy, Z. Chen, M. Schoenauer Sebag, Z. Hu, X. Xu, L. Billot, L. Aigouy and Z. Chen, *Small*, 2018, **14**, 1704013.

35 G. C. FOSTER, *Nature*, 1894, **50**, 399.

36 C. R. Barber, *J. Sci. Instrum.*, 1950, **27**, 47–49.

37 V. Batagelj, J. Bojkovski and J. Drnovšek, *Meas. Sci. Technol.*, 2003, **14**, 2151.

38 N. Miyakawa, W. Legner, T. Ziemann, D. Telitschkin, H.-J. Fecht and A. Friedberger, *Microsyst. Technol.*, 2012, **18**, 1077–1087.

39 L. Aigouy, P. Lalanne, J. P. Hugonin, G. Julié, V. Mathet and M. Mortier, *Phys. Rev. Lett.*, 2007, **98**, 153902.

40 E. Saïdi, N. Babinet, L. Lalouat, J. Lesueur, L. Aigouy, S. Volz, J. Labéguerie-Egéa and M. Mortier, *Small*, 2011, **7**, 259–264.

41 H. Xiang, T. Niu, M. Schoenauer Sebag, Z. Hu, X. Xu, L. Billot, L. Aigouy and Z. Chen, *Small*, 2018, **14**, 1704013.

42 K.-J. J. Kim, J.-C. C. Lee, S.-B. B. Choe and K.-H. H. Shin, *Appl. Phys. Lett.*, 2008, **92**, 192509.

43 C. V Hoang, K. Hayashi, Y. Ito, N. Gorai, G. Allison, X. Shi, Q. Sun, Z. Cheng, K. Ueno, K. Goda and H. Misawa, *Nat. Commun.*, 2017, **8**, 771.

44 A. Pescaglini, A. Martín, D. Cammi, G. Juska, C. Ronning, E. Pelucchi and D. Iacopino, *Nano Lett.*, 2014, **14**, 6202–6209.

45 Z. Sun, L. Aigouy and Z. Chen, *Nanoscale*, 2016, **8**, 7377–7383.

46 P. K. Jain, X. Huang, I. H. El-Sayed and M. A. El-Sayed, *Acc. Chem. Res.*, 2008, **41**, 1578–1586.

47 M. R. K. Ali, M. A. Rahman, Y. Wu, T. Han, X. Peng, M. A. Mackey, D. Wang, H. J. Shin, Z. G. Chen, H. Xiao, R. Wu, Y. Tang, D. M. Shin and M. A. El-Sayed, *Proc. Natl. Acad. Sci.*, 2017, **114**, E3110–E3118.

48 G. von Maltzahn, J.-H. Park, A. Agrawal, N. K. Bandaru, S. K. Das, M. J. Sailor and S. N. Bhatia, *Cancer Res.*, 2009, **69**, 3892 LP – 3900.

49 Q. Chen, Q. Chen, H. Qi, L. Ruan and Y. Ren, *Nanomaterials*, 2017, 7, 416.

50 Z. H. Chen, Y. B. Tang, C. P. Liu, Y. H. Leung, G. D. Yuan, L. M. Chen, Y. Q. Wang, I. Bello, J. A. Zapien, W. J. Zhang, C. S. Lee and S. T. Lee, *J. Phys. Chem. C*, 2009, **113**, 13433–13437.

51 A. Sobhani, A. Lauchner, S. Najmaei, C. Ayala-Orozco, F. Wen, J. Lou and N. J. Halas, *Appl. Phys. Lett.*, 2014, **104**, 031112.

52 F. Pelayo García de Arquer, F. J. Beck, M. Bernechea and G. Konstantatos, *Appl. Phys. Lett.*, 2012, **100**, 043101.

53 G. E. Stillman, C. M. Wolfe and I. Melngailis, *Appl. Phys. Lett.*, 1974, **25**, 36–38.